Polymer Journal (2019) 51:143–153
https://doi.org/10.1038/s41428-018-0128-5

ORIGINAL ARTICLE

Synchrotron microbeam X-ray scattering study of the crystallite orientation in the spherulites of isotactic poly(butene-1) crystallized isothermally at different temperatures

Kohji Tashiro[1] · Hiroko Yamamoto[1,3] · Kenichi Funaki[2] · Jian Hu[1,4]

Received: 18 July 2018 / Revised: 30 August 2018 / Accepted: 3 September 2018 / Published online: 5 November 2018
© The Society of Polymer Science, Japan 2018

Abstract

The hierarchical structure of spherulites grown isothermally from a melt was investigated for isotactic poly(butene-1) (*it*-PB-1) by analyzing wide-angle and small-angle X-ray scattering data measured simultaneously at various positions of the spherulites using a synchrotron X-ray microbeam technique. In square-shaped spherulites (hedrites) grown at 103 °C, the chain axis stands along the direction normal to the spherulite surface and the *a* and *b* axes of the original form II crystal direct in parallel to the square edges. On the other hand, for round-shape spherulites grown at 98 °C, the chain axis lies tangentially along the circle of the round spherulite surface. These spatial geometries, revealed by the X-ray microbeam method, have confirmed previously-reported results that were qualitatively derived from 2-dimensional polarized FTIR imaging experiments [J Phys Chem B. 2016;120:4689]. Surprisingly, only a 5 °C difference in the isothermal crystallization temperature gives rise to remarkably different hierarchical structures of *it*-PB-1, as clarified by the X-ray microbeam technique.

Introduction

When a crystalline polymer is cooled slowly or isothermally from the melt, spherulites are generally formed with diameters in the μm–mm range. The spherulites are composed of aggregations of the crystalline lamellae, which grow radially from the spherulite center. The hierarchical structure information or the spatial relation between the inner-structure of the crystal lattice, the orientation of crystalline lattices in the lamella, the stacking mode of these lamellae and the morphology of the whole spherulite is indispensable for understanding the formation mechanism of the spherulites.

In the present paper, we focus on the spherulites of *isotactic* poly(butene-1) [*it*-PB-1, -$(CH_2CH(CH_2CH_3))_n$-]. The reason for choosing this polymer is that *it*-PB-1 shows various crystalline forms (I, II, III, etc.) depending on the sample preparation conditions [1–40], and the external shape or morphology of the spherulites grown from the melt is sensitively varied depending on the crystallization temperature [30–40]. For example, the isothermal crystallization at 103 °C gives spherulites that have a square shape, while round-shaped spherulites are observed at 98 °C, only a slightly lower temperature. The single-crystal-like platelets of polygonal appearance are called hedrites [41]; however, in the present paper, the products having a square or round shape, created at the different temperatures, are termed spherulites. In the *it*-PB-1 spherulites grown at a high temperature (near 100 °C), the crystalline form II is crystallized, but the morphology or the outer shape of the

✉ Kohji Tashiro
ktashiro@toyota-ti.ac.jp

[1] Department of Future Industry-Oriented Basic Science and Materials, Toyota Technological Institute, Tempaku, Nagoya 468-8511, Japan

[2] Toyobo Research Center, Toyobo Co. Ltd., 2-1-1 Katata, Ohtsu 520-02, Japan

[3] Present address: Aichi Synchrotron Radiation Center, Aichi Science and Technology Foundation, 250-3 Minamiyamaguchi, Seto 489-0965, Japan

[4] Present address: Department of Key Laboratory of Rubber-Plastics (QUST), Ministry of Education Room 304, Qingdao University of Science and Technology, Shibei, Qingdao 266042, China

spherulite is quite different between 98 °C and 103 °C. It is important to investigate the difference in the hierarchical structure of these different types of spherulites obtained at only slightly different temperatures. In a series of papers [7, 42, 43] we investigated the crystal structures and higher-order structures of *it*-PB-1 using wide-angle X-ray diffraction (WAXD) and small-angle X-ray scattering (SAXS) techniques mainly. Additionally, we used a polarized FTIR imaging technique to study the inner structure of the spherulites [44]. Below, we will briefly review the structures of the representative crystal forms I and II of *it*-PB-1 in regards to the basic knowledge of the hierarchical structure of spherulites.

Crystal structure of forms I and II

The crystalline forms I and II are the most popular modifications of *it*-PB-1. Crystallization from the melt generates form II, which transforms spontaneously to form I by cooling to room temperature. Stretch of the form II accelerates this transformation. For this reason, the highly oriented and pure form II sample was quenched in liquid nitrogen immediately after preparation, and the X-ray diffraction pattern was measured using a flow of cold nitrogen gas to suppress the transformation to form I [42]. By analyzing the collected 2D X-ray diffraction pattern, the crystal structure of form II was determined, as shown in Fig. 1a. Form II takes the tetragonal unit cell of $a = b = 14.9$ Å and c (chain axis) $= 21.3$ Å, with the space group $P\overline{4}b2$. The molecular chain takes the (11/3) helical conformation, and the right-handed (R) and left-handed (L) chains are alternately packed within the cell. The 2D X-ray diffraction pattern of the oriented form I was measured by using the oriented form II sample left at room temperature for a long time. The X-ray data analysis gave the structure shown in Fig. 1b, where the unit cell parameters are $a = b = 17.53$ Å, c (fiber axis) $= 6.477$ Å and $\gamma = 120^{o}$, and the space group symmetry is $P\overline{3}$. The chain conformation of form I is a (3/1) helix, where three monomeric units rotate by one turn in the repeating period (c). The R and L helices are alternately packed in the hexagonal unit cell. The key point to estimate the transition mechanism is to find the common features of the chain packing mode between these two crystal forms. In both crystal forms I and II, the upward and downward chains are located randomly at a lattice site with 50% probability. Additionally, the diagonal direction of the *ab* plane or the 110 direction is kept in the structural transformation (Fig. 1c), as is known from the electron diffraction data of the single crystal [13, 26, 42, 45]. The phase transition was proposed to occur in a type of soft mode, that is, the translational lattice vibrational mode of the R and L chains with the phase angle π being anharmonically softened. The R and L helical chains in the tetragonal unit cell translate in an opposite direction along the 110 plane cooperatively, and they are stabilized into the unit cell of form I [42].

Inner structure of spherulites

As seen from the optical microscopic observations, the spherulites of *it*-PB-1 grown from the melt have a different morphology depending on the isothermal crystallization temperature [33–39]. As shown in Fig. 2, isothermal crystallization in the high-temperature region, approximately 20 °C lower than the melting point (approximately 125 °C), results in spherulites with a regular square shape; this reflects the tetragonal unit cell of form II. However, spherulites with a round shape are obtained when crystallization is carried out at 98 °C, only 5 °C lower than the case of square spherulites. By utilizing the 2D-imaging FTIR microscope technique [46–48], we measured the polarized IR spectra at various points of the spherulites and obtained 2D images showing the spatial distribution of the molecular chain orientation [44].

In the square-shaped spherulites grown at 103 °C, the crystallites are of the form II and the chain axis stands perpendicularly to the spherulite surface. The a and b axes were found to be parallel to the spherulite edges. On the other hand, in the case of 98 °C crystallization, the c axis lies on the spherulite surface and distributes circularly around the center, while the a (b) axis stands vertically. In this way, the polarized IR microscope gave us detailed information about the spatial orientation of the crystal lattice in forms I and II.

However, the polarized IR microscope cannot give us more concrete and detailed information about the aggregation state of the crystalline lamellae. Furthermore, the discussion remains semi-qualitative as long as we use only the relative intensity of the perpendicularly-polarized and parallel-polarized IR band components. We need to know the 3-dimensional crystallite orientation and the aggregation structure of the lamellae in the spherulites in more detail. This information may be obtained by performing X-ray scattering experiments. WAXD can give us the information on the 3D-spatial orientation of the unit cell. SAXS data can reveal the aggregation of the stacked lamellae in the spherulites. Of course, the WAXD and SAXS data must not be collected separately, but they should be measured at the same position and at the same time because the position of the incident X-ray beam is extremely difficult to control for a tiny spherulite. Additionally, the usage of the large-size X-ray beam, several hundred micrometers in diameter, cannot give us details about the local structure distribution, but only structural information averaged over the wide range of the sample. To clarify the spatial distribution of the crystallites and lamellae at a higher resolution, we need to use

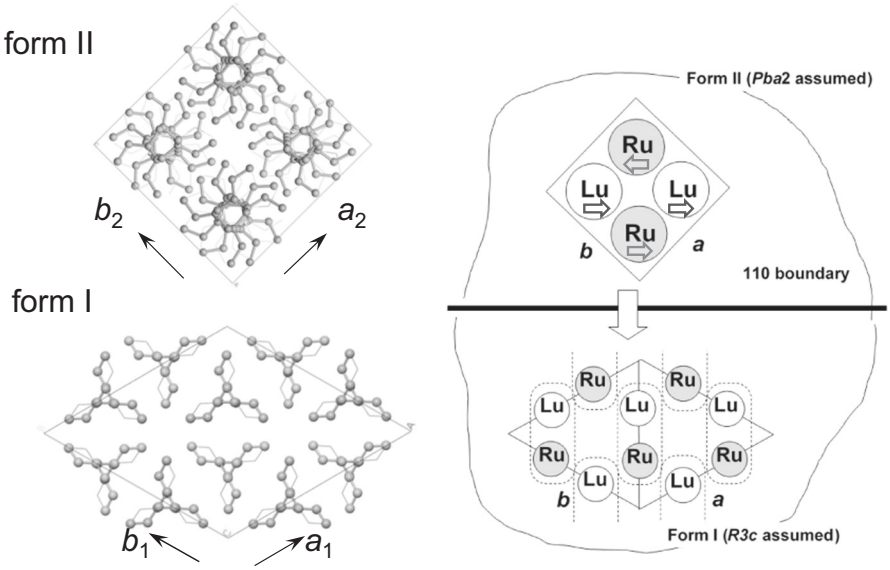

Fig. 1 Crystal structures of *it*-PB-1 forms II and I, and an illustration of the phase transition between them through the translational motions into the opposite directions along the 110 plane [42]. The translational shift along the vertical direction causes the formation of the other orientation of the form I unit cell (refer to Fig. 5). In other words, there is a twinned structure of form I

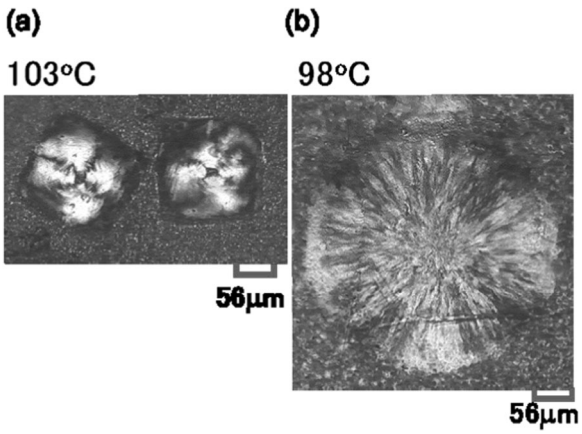

Fig. 2 Spherulites of *it*-PB-1 obtained by isothermal crystallization at **a** 103 °C and **b** 98 °C, followed by cooling to room temperature

the so-called X-ray microbeam or an X-ray beam focused to a micrometer size. However, an X-ray beam that is a few micrometers in diameter, produced by a laboratory-level X-ray generator, is too weak to detect diffraction data with a high enough S/N ratio. We need to utilize a more brilliant synchrotron X-ray source for the production of a micrometer-sized X-ray beam that has a higher brilliance [49–53].

By taking into account all of the abovementioned situations, we simultaneously and systematically measured a series of 2D WAXD and SAXS patterns at various local positions of *it*-PB-1 spherulites using an X-ray microbeam produced from a highly brilliant synchrotron radiation system. The use of a synchrotron X-ray microbeam for round-shaped *it*-PB-1 spherulites was reported by Toda et al. [49]. However, a detailed analysis was not successfully performed, as they themselves noted in their report. Furthermore, they did not measure the SAXS data in parallel with the WAXD measurements. In the present paper, we simultaneously measured the WAXD and SAXS patterns for the two different types of *it*-PB-1 spherulites. These data were quantitatively interpreted to reveal the hierarchical structures of these two spherulites. As noted above, the inner structure and outer shape of the *it*-PB-1 spherulites can easily change due to small changes in the isothermal crystallization temperature. The X-ray data analysis not only confirmed the structural images deduced from the semi-quantitative 2D-imaging FTIR microscopic study but also revealed more detailed information on the inner structure of the spherulites.

Experimental section

Samples

The *it*-PB-1 sample used here was supplied by Mitsubishi Chemicals, Japan. The averaged molecular weight was 110 kg/mol and the triad isotacticity was approximately 98%. The sample was melted at approximately 160 °C on a KBr single-crystal plate and then cooled immediately to a predetermined temperature (*T*c) and kept for a long time so that the spherulites grew to a sufficient size. The *T*c values chosen here were 103 and 98 °C, the same temperatures that were utilized in the 2D IR imaging experiment, as reported in the previous paper [44]. The obtained spherulites were cooled quickly to room temperature and taken out of the KBr plates by immersing into a water bath.

Measurements

Here, the spherulite samples used in the X-ray diffraction measurements were not of the thus-prepared crystalline form II, but rather the samples consisted of form I crystallites, since the samples were left at room temperature for a long period of time. However, the use of these spherulite samples can be accepted here because our aim is to clarify the spatial relation between the aggregation state of the crystallites and the stacked lamellar structure. As already reported, we know that (i) the chain axis direction is maintained even after the phase transition from form II to form I; and (ii) the diagonal [110] direction is common to both forms I and II and is maintained unchanged during the phase transition (Fig. 1c). Therefore, the crystallographic geometry deduced by the quantitative X-ray data analysis performed for the form I lamellae is assumed to be the same as that in the high-temperature state consisting of the crystal form II, although the crystal structure including the chain conformation and chain packing mode is different between these two crystal forms. In other words, we can speculate on the crystallization behavior of form II crystals at a high temperature through the analysis of the form I crystals at room temperature. Another reason why we used the spherulites left at room temperature is the difficulty of the repeated X-ray diffraction measurements at the various positions of a spherulite in the crystallization process at a high temperature, although this would be an interesting and important research theme. The irradiation of the brilliant synchrotron X-ray microbeam damaged the sample after exposure for several seconds, making it impossible to scan the X-ray beam at the same positions many times during the growth of the spherulite at a high temperature. The laboratory X-ray microbeam is too weak to trace the structural change in the spherulite. The reason for the 2D FTIR imaging experiment, as reported previously, was a result of this situation.

The present paper investigates the inner structure of the spherulites left at room temperature using a synchrotron X-ray microbeam method, and the obtained results may be a good monitor for estimating the structural situation of the spherulites in crystallization processes at a high temperature, since the hierarchical structure is retained.

The WAXD/SAXS simultaneous measurements were performed at beam line 03XU in SPring-8, Japan. A snapshot of the measurement system is shown in Fig. 3. The X-ray beam size, which was controlled using a Fresnel Zone Plate, was 1.4 (horizontal) × 1.1 (vertical) μm^2 (half widths). The spherulite sample was set on the XZ stage and shifted stepwise along the vertical and horizontal directions at the 10 μm pitch (for the spherulite grown at $Tc = 98$ °C) or 20 μm pitch (for the spherulite grown at $Tc = 103$ °C) in the range of 400 μm width. The X-ray wavelength was 1.305 Å. The flat panel detector (C9728-DK, Hamamatsu Photonics) set approximately 40 mm from the sample position was used for the WAXD measurement. The CCD detector (C4742-98, Hamamatsu Photonics) with an Image-intensifier (V7735P, Hamamatsu Photonics) was used for the SAXS data collection at a camera distance of 600 mm. The X-ray exposure time was 2 s per shot. The X-ray beam position on the sample was monitored by observing the spherulite image on the video camera display.

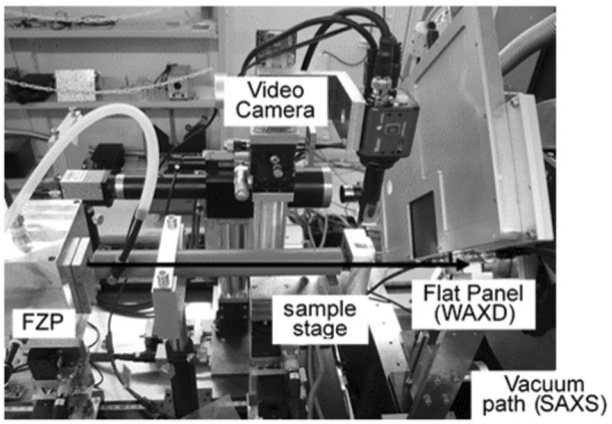

Fig. 3 Synchrotron X-ray microbeam experimental system. FZP Fresnel zone plate. The image-intensifier-CCD detector for the SAXS data collection was set to approximately 600 mm behind the sample stage after passing through the vacuum pipe

Results and discussion

Spherulites grown at 103 °C

Figure 2a shows the polarized optical microscopic image of the spherulites (hedrites) isothermally grown at 103 °C from the melt. Even after completion of the phase transition from form II to form I at room temperature, the spherulite shape is apparently square, almost the same as that observed at 103 °C, although the inner structure is filled with the crystalline form I in addition to the amorphous region (the reason for this situation will be mentioned in a later section). The optical microscope images are not very homogeneous compared with those taken at 103 °C because of the phase transition from form II to I, giving a twinned structure, as explained later. The WAXD and SAXS patterns measured at the various positions of the spherulite are shown in Figs. 4–6, where the X-ray beam was incident perpendicularly to the spherulite surface. In Fig. 4, the observed WAXD patterns were found to be essentially the same for the various measurement positions. All the observed reflections were indexed using the unit cell parameters of the form I, as indicated on the diffraction pattern in Fig. 4. We immediately noticed that only the *hk*0

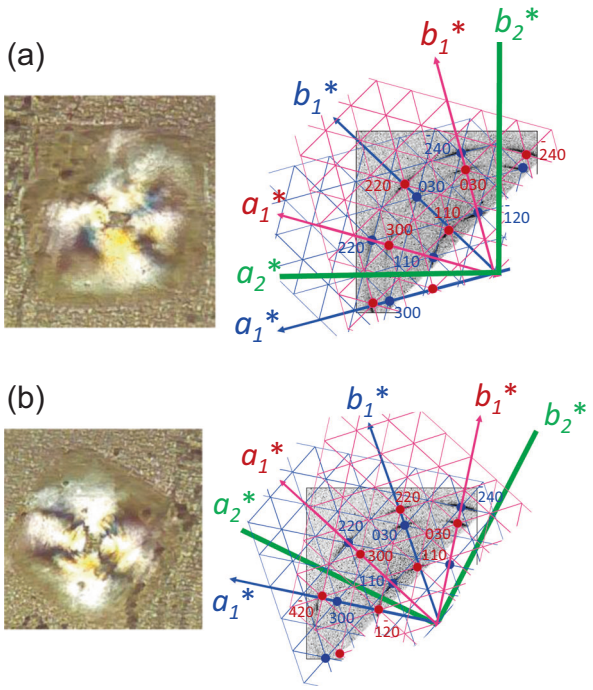

Fig. 4 Indexing of the WAXD patterns measured for the spherulites grown at 103 °C. The red and blue axes are for crystal form I. The green lines correspond to the unit cell axes of crystal form II and are parallel to the edges of the square spherulites. Cases (**a**) and (**b**) are presented here to demonstrate the correct indexing for the WAXD patterns obtained for the different spherulites (refer to Fig. 2)

reflections were observed for the spherulites grown at 103 °C, indicating the orientation of the chain axis perpendicular to the spherulite surface.

A more detailed analysis of the WAXD patterns shown in Fig. 4 was carried out. As mentioned above, all the observed reflections were successfully indexed as *hk*0 spots of the form I crystal; however, they were found to consist of the overlap of many sets of the reciprocal a_1* and b_1* axes, as indicated by the red and blue colors in Fig. 4 (the subscript "1" indicates the form I crystal). In case (a), the green median line between the a_1* (red) and a_1* (blue) axes is parallel to the edge of the square spherulite. In case (b), the situation is the same, although the edges are tilted slightly from the horizontal axis. Originally, the square edge came from the edge of the square-shaped spherulite of crystalline form II. The correspondence between the green edge lines and the a_1* and b_1* axes of the red and blue colors should be consistent with the structural relationship between the forms II and I in the phase transition. The electron diffraction data indicated that the [110] direction is their common axis. In the phase transition, the form II unit cell of the perfectly square shape is deformed to a lozenge shape of the form I cell, just when the two types of the mutually perpendicular deformation may occur because of the crystallographic equivalency of the a_2 and b_2 axes. That is to say, the twinned structure with the perpendicular orientations as shown in Fig. 5d is formed by the sliding motion of the chain stems along the 110 or $1\bar{1}0$ planes. The overlap of the form I unit cells (red and blue colors in Fig. 4) with the 30° different orientation angles arises from such a transition mechanism. The WAXD data of Fig. 4 reflects these complicated situations. Once we know the structural relationship between the crystal lattices and the spherulite edges, we can immediately speculate that the crystal grows along the [110] direction with the formation of the alternate array of the folded chain planes of the R and L chain stems, as illustrated in Fig. 5a, b.

The results of the SAXS data are presented in Fig. 6. No clear peak was observed at any position on the large spherulite. On the other hand, a ring pattern with spacing of approximately 155 Å was observed when the X-ray beam was incident on the positions outside the main spherulite. This peak corresponds to the second-order component of the stronger peak detected at the position close to the beam stopper, and the long period should be approximately 310 Å, which is consistent with the previously reported values [40, 43]. The spherulites detected outside are quite small; these were grown in the rapid cooling process from *Tc* to room temperature. The WAXD pattern also gave Debye-Scherer rings, meaning that the outside tiny crystallites orient into various directions. According to the SAXS pattern of the main square-shaped spherulite, we can conclude that the crystalline lamellae are stacked with the normal directing perpendicularly to the spherulite surface (the flat-on orientation).

Figure 5a shows an illustration of the deduced lamellar stacking structure with the crystal lattice orientation. The molecular chains orient vertically on the spherulite surface, and the [110] directions are along the diagonal lines of the square. In this figure, the lamellar stacking structure with the chain folding is also included, as explained above. The originally generated form II crystal possesses tetragonal symmetry, resulting in the square shape of the spherulite.

Spherulites grown at 98 °C

Figure 7 shows the WAXD patterns measured for the spherulites grown at 98 °C. The X-ray beam was incident along the normal to the spherulite surface. Similar patterns were observed at various positions of the spherulite. As shown in Fig. 7b, all the observed 2D diffraction patterns are reasonably interpreted by referring to the fiber pattern of the uniaxially oriented sample consisting of the 0th, 1st, and 2nd layer lines [42]; the c* axis is perpendicular to the reflection layer lines, indicating that the c axis lies on the surface. The observed WAXD patterns are essentially the same at the various positions, but the c* axis always

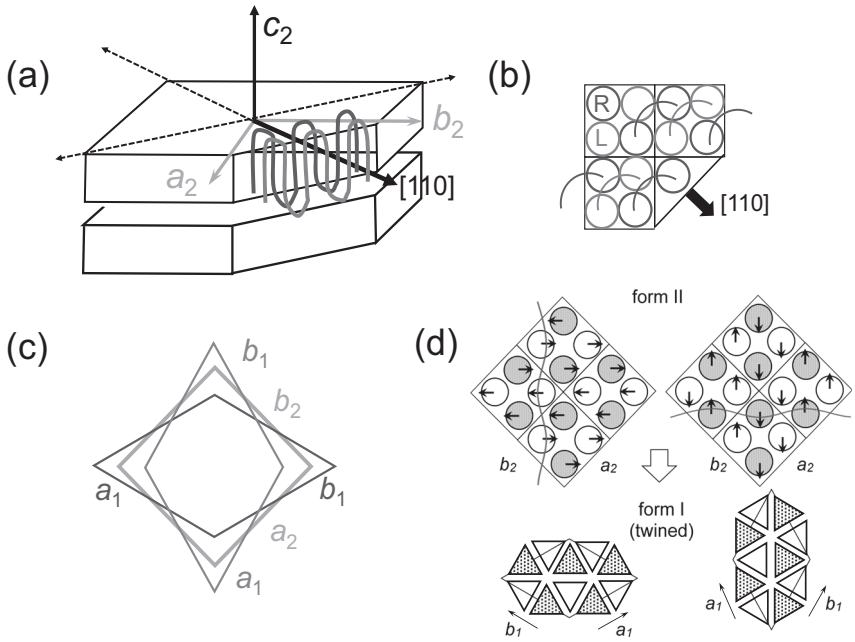

Fig. 5 **a**, **b** Illustrations of the inner structure of the spherulites grown at 103 °C. The crystal axes of the original form II are shown here. The chain folding occurs along the 110 plane. **c** The relation of the crystal axes between forms I and II. A twinned structure is possible for form I, as seen in the illustration (**d**)

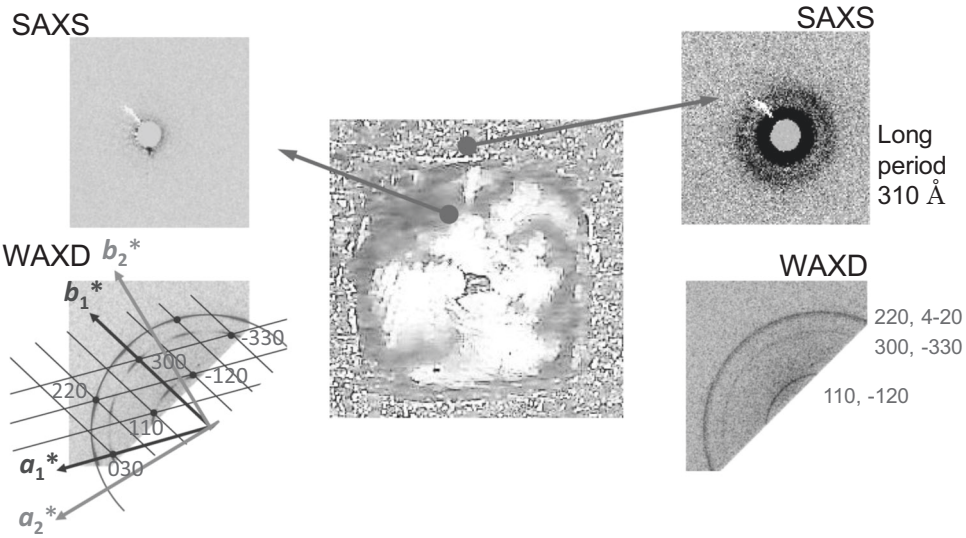

Fig. 6 SAXS and WAXD patterns measured at different positions of the square-shaped spherulite of *it*-PB-1 grown at 103 °C. The SAXS and WAXD patterns detected outside are ring patterns, indicating the tiny spherulites orienting into the various directions

directs toward the tangential direction of the spherulite circle (Fig. 7a). The observed diffractions show appreciably long arcs (corresponding to an approximately 30° azimuthal angle), suggesting the relatively poor orientation of the c^* axis. One reason for this might come from the finite size of the incident X-ray beam, which has an approximately 1.2 μm radius. The irradiated X-ray beam covers the spherulite local area of the 1.2 μm radius from which the diffraction occurs. The c^* axis included in the range of the 1.2 μm radius is estimated to orient in the range of ±1° around a position 100 μm distant from the spherulite center. This is too small compared with the observed arc length. The long arc may reflect orientational fluctuation of the c axis, as will be discussed later.

Determining the directions of the a^* and b^* axes around the c^* axis is also rather ambiguous. As seen in Fig. 7, the X-ray beam is incident from the direction that is normal to the spherulite surface. Notably in the observed WAXD pattern, the 110, 300, and 220 Bragg reflections are detected in one X-ray diffraction pattern, indicating that the crystal orients so that all these corresponding reciprocal lattice points cross the Ewald sphere. As illustrated in Fig. 8, one possible orientation is that the a^* axis is on the surface, in other words, the b axis stands vertically to the spherulite surface. The green curve is a so-called Ewald sphere. The 300 reciprocal lattice point crosses the Ewald sphere. In order for the 110 and 220 reflections to be observed at the same time, the reciprocal lattice plane must rotate around

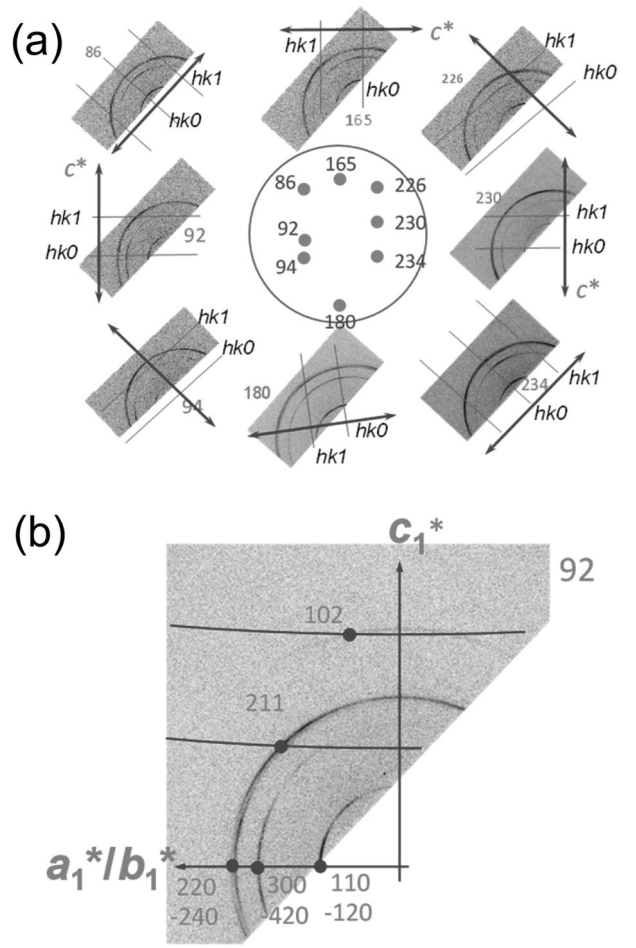

Fig. 7 **a** WAXD patterns measured at various positions of the *it*-PB-1 spherulites grown at 98 °C. The blue lines indicate the direction of the *c** axis, which orients circularly around the spherulite center. **b** Indexing of the observed reflections. The numbers added to the WAXD patterns indicate the X-ray irradiation positions on the spherulite

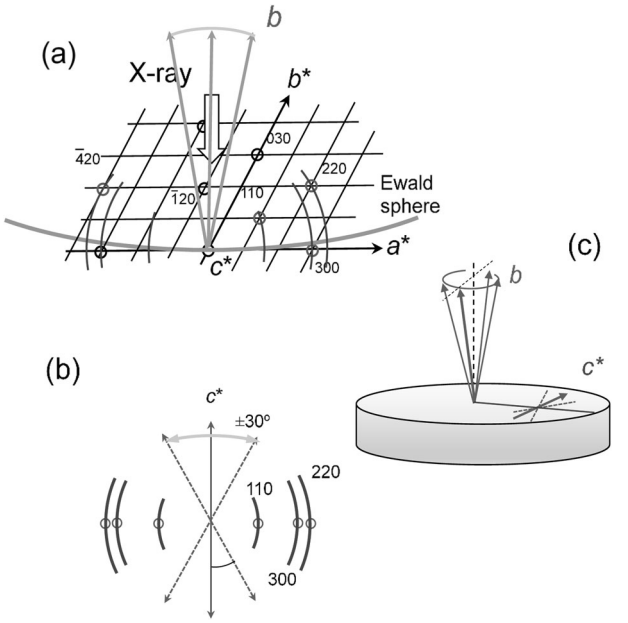

Fig. 8 **a** Explanation of the observation of 110, 300, and 220 reflections. The corresponding reciprocal lattice points must contact the Ewald sphere by an approximately 30° rotational fluctuation of the *c** axis. In this figure, the *a** axis is assumed to be on the spherulite surface. **b** The misorientation of the *c** axis from the tangential direction of the circle. **c** An illustration of the *b* and *c* axial orientations on the spherulite plane

the *c** axis by approximately ±30°. Another possibility is that the 110 and 220 axes are on the horizontal plane. The 30° fluctuation around the *c** axis causes the 300 reflection to cross the Ewald sphere. In the present data, it is difficult to distinguish these two possibilities. The true situation might be between these two possibilities. At the same time, we need to consider the long arc lengths of these reflections, as previously noted in Fig. 7. This means that the *c** axis also fluctuates by ±30° from the ideal direction (see Fig. 7b). In this way, the unit cell axes are speculated to fluctuate their orientations by approximately ±30° from such an ideal direction that the *a** axis is included in the spherulite surface and that the *c** axis directs to the tangential direction of the round edge of the spherulite.

The fluctuation of the *c** axial direction is intimately related to the SAXS pattern. The observed SAXS patterns are shown in Fig. 9. The log period peaks (the second-order peaks) are observed in the direction parallel to the *c** axis (red arrows), indicating that the lamellae are stacked along the *c** axis with a long period of approximately 380 Å. (The strong meridional scattering was detected quite close to the beam stopper, and the clear peak detected in Fig. 9 should correspond to the second-order peak.) In more exact terms, the meridional direction giving the SAXS peaks is not perfectly parallel between the neighboring positions, but fluctuates similarly to the *c** axis (refer to Fig. 8).

By combining the WAXD and SAXS data, the lamellae are speculated to grow with a curved shape in the radial direction, as illustrated in Fig. 10, where the above-mentioned orientational fluctuation of the *b** (*a**) axis around the *c** axis is ignored for simplicity. This curved lamellar image is quite different from the so-called lamellar twisting mode, in which the lamellae grow radially, with a 180° rotation around the radial axis [54–63]. If the lamellae of *it*-PB-1 are twisted around the radial direction, the periodic ring pattern must be detected on the spherulite image [49]. Such a ring pattern was not detected in the spherulites of *it*-PB grown at 98 °C. This conclusion is consistent with the report of the polarized 2D IR imaging.

Morphology and hierarchical structure

As discussed above, the relation between spherulite morphology, lamellar orientation and crystallite orientation has been clarified by the interpretation of the observed WAXD

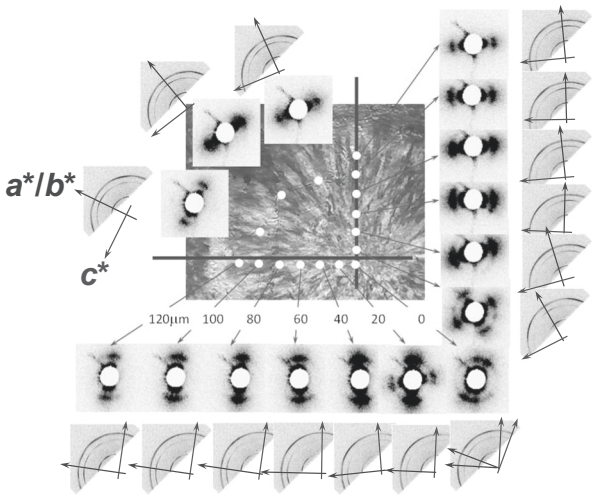

Fig. 9 SAXS and WAXD patterns measured at various positions of the *it*-PB-1 spherulites grown at 98 °C. The blue lines indicate the direction of the equatorial *hk*0 reflection line. The red lines indicate the *c** axial directions, which are parallel to the direction of the meridional scattering peaks of the SAXS patterns. The clearly observed SAXS peak is the second-order peak of the stronger 1st-order peak that is partially hidden by the beam stopper

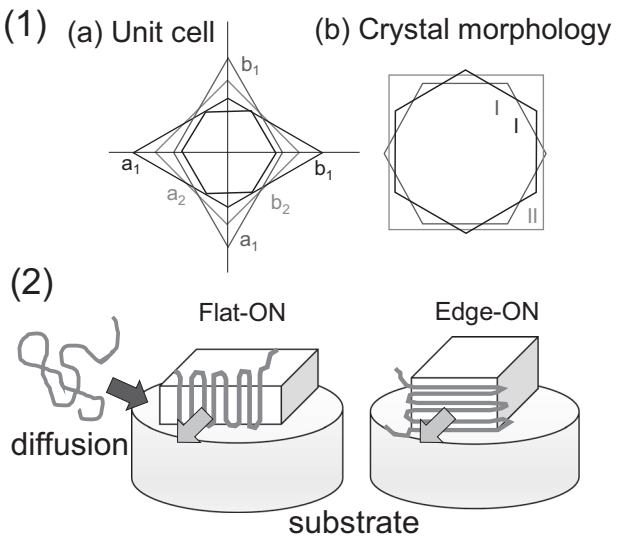

Fig. 11 (1) Relation of the unit cell and morphology between crystal forms I and II. The form I takes a twinned structure. The external shape of the crystal, as shown in the right side, was calculated with the BFDH method [64], which is nearly the same between the two forms. (2) Illustration of flat-on and edge-on structures of the lamellae on the substrate

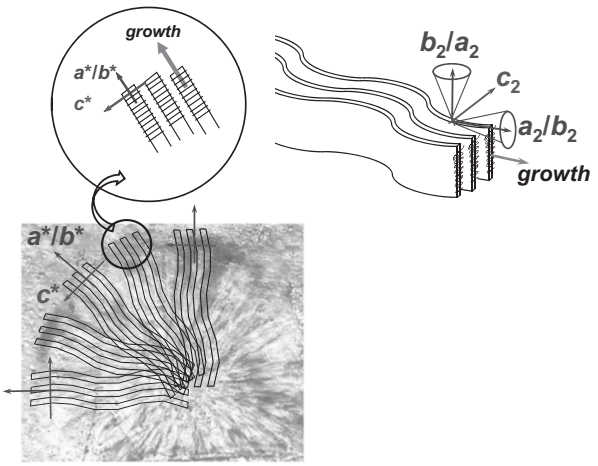

Fig. 10 Illustration of the stacked lamellar structure for the *it*-PB-1 spherulites grown at 98 °C. The lamellae are curved along the growth direction from the center. The *c* axis is perpendicular to the lamellar surface. The *a* and *b* axes of the original form II crystal are shown here, which fluctuate from the vertical direction

and SAXS patterns of the samples grown at 103 °C and 98 °C. Several points should be considered here regarding the structural features of these spherulites.

Morphology

As mentioned above, the morphology or external shape of the spherulite hardly changed before and after the phase transition from the high-temperature form II to the low-temperature form I. For the spherulites grown at 103 °C, the unit cell of form II takes a square shape, while that of form I is triangular (or lozenge). The square shape of the spherulites observed even after the transition to form I appears to be inconsistent with the shape of the form I unit cell. The morphology was predicted from the unit cell structure on the basis of the BFDH method (Bravais-Friedel-Dannay-Harker method, [64]) using the commercial software Materials Studio (Biovia, version 2017R2), which assumes that crystal growth occurs by adding crystal planes to the existing plane and that the growth rate is higher for thinner planes or those having a shorter lattice spacing. Additionally, the morphology was calculated with the equilibrium morphology method [65], in which the planes with the minimal surface energy are searched, but the results were essentially the same as those from the BFDH method. The predicted external shape of the crystal lattice is shown for the tetragonal and hexagonal lattices in Fig. 11 (1). To draw the polyhedrons, their relative sizes were calculated by assuming that the total number N of the molecular chain stems in the polyhedron is the same, but the effective cross-sectional area of a chain stem is different between forms I and II. For the edge length A_2 of the square, the cross-sectional area is $A_2{}^2 = N^* a_2{}^2/4$, since the 4 chain stems are included in the unit cell of form II with the unit cell length a_2 (Fig. 1), while the cross-sectional area of the hexagon with the edge length A_1 is $(3\sqrt{3}/2)A_1{}^2$, which should be equal to the total area of the N chain stems $= N^* a_1{}^2 \sin(120^o)/6 = (\sqrt{3}/12)a_1{}^2 N$ (6 chain stems are included in the unit cell of the form I crystal, where a_1 is the unit cell

length). Therefore, the ratio of the edge length $A_1/A_2 = 2a_1/(\sqrt{18}a_2)$. Since form I takes a twinned structure, the two types of hexagon are possible, with orientations differing by 90°. The conclusion is that the rough shape is maintained nearly unchanged between these two spherulites, except for the corner parts, as seen in Fig. 11 (1).

Flat-on and edge-on orientations of molecular chains

As illustrated in Figs. 5 and 10, the orientation of the chain stems and the stacking of the lamellae are different depending on the preparation temperature; flat-on occurs in the 103 °C spherulites and edge-on occurs in the 98 °C spherulites (see Fig. 11). There has been some debate regarding the growing mechanism of the lamellae. Some of the key factors are the interaction of molecular chains with the substrate, the thermally induced sliding motion of chains confined in an extremely thin film, the role of the intermediate phase with the disordered packing structure of thermally activated chains, the nucleation rate on the substrate and so on [66]. In the present case, crystallization occurs on the same KBr platelet for the same *it*-PB-1 sample with the same molecular weight. Some of the abovementioned factors may play a role to give the remarkably different chain orientations seen in spherulites grown at temperatures that differ by only 5 °C. However, the driving forces causing such different lamellar aggregation states remain unknown.

Conclusions

In the present paper the hierarchical structure of the spherulites of *it*-PB-1 has been successfully investigated in detail through the step-scanned simultaneous measurements of the WAXD and SAXS 2D-patterns at various positions using a synchrotron X-ray microbeam. Although the X-ray data were collected for the spherulites of form I obtained by cooling the form II crystals to room temperature, the hierarchical structure remains unchanged even after the transition from form II to I, allowing us to estimate the inner structure of the spherulite at a high temperature by carefully analyzing the observed X-ray data. The spherulite morphology of *it*-PB-1 is sensitive and changes depending on the isothermal crystallization temperature. The square shape of the spherulites grown at 103 °C arises from the tetragonal symmetry of the form II. The lamellae are stacked in a flat-on mode on the spherulite surface without any twisting. The *c* axis stands vertically on the spherulite surface. The *a* and *b* axial directions of the original form II crystals are parallel to the square edges. On the other hand, the spherulites grown at 98 °C show a round shape. Their chain axis lies on the surface and orients tangentially along the spherulite circle. The *b* axial orientation fluctuates by approximately ±30° around the direction that is normal to the surface. The lamellae exist in the edge-on mode and grow radially with the fluctuation of the *c*-axial orientation within the surface. These results, derived from the microbeam X-ray scattering experiments, are consistent with the previously reported 2D FTIR microscopic study.

The X-ray microbeam is a powerful technique used to trace the hierarchical structure of a tiny spherulite, although the beam size is still large for a more detailed study of the local structure at the sub-nanometer scale. The growing mechanism of spherulites is still a controversial topic. The accumulation of microbeam WAXD/SAXS data for various types of spherulites might further accelerate research of the complicated hierarchical structure of crystalline polymers.

Acknowledgements The synchrotron radiation experiments were performed at the BL03XU of SPring-8 with the approval of the Japan Synchrotron Radiation Research Institute (JASRI). This study was financially supported by MEXT "Strategic Project to Support the Formation of Research Bases at Private Universities (2010-2014 and 2015-2019)".

Compliance with ethical standards

Conflict of interest The authors declare that they have no conflict of interest.

References

1. Luciani L, Seppälä J, Löfgren B. Poly-1-butene: its preparation, properties and challenges. Prog Polym Sci. 1988;13:37–62.
2. Natta G, Pino P, Corradini P, Danusso F, Mantica E, Mazzanti G, Moraglio G. High Polymers of α-Olefins. J Am Chem Soc. 1955;77:1708–10.
3. Natta G, Pino P, Mazzanti G, Corradini P, Giannini U. Synthesis and properties of crystalline high polymers of branched α-olefins. Rend Accad Naz Lince-. 1955;19:404.
4. Natta VG, Corradini P, Bassi IW. uber die Kristallstriiktur des Isotaktischen Poly-α-butens. Die Makromol Chem. 1956;21:240–4.
5. Natta G, Corradini P, Bassi IW. Crystal structure of isotactic poly-alpha-butene. Nuovo Cim Suppl. 1960;15:52–67.
6. Miller R, Nielsen L. Crystallographic Data for Various Polymers II. J Polym Sci. 1961;55:643–56.
7. Tashiro K, Asanaga H, Ishino K, Tazaki R, Kobayashi M. Development of a new software for the X-ray structural analysis of polymer crystals by utilizing the X-ray imaging plate system. J Polym Sci Part B Polym Phys. 1997;35:1677–1700.
8. Turner AJ. Polybutene-1-type II crystalline form. J Polym Sci Part B Polym Phys. 1963;1:455–6.
9. Miller RL, Holland VF. On transformations in isotactic polybutene-1. J Polym Sci Part B Polym Lett. 1964;2:519–21.
10. Petraccone V, Pirozzi B, Frasci A, Corradini P. Polymorphism of isotactic poly-α-butene conformational analysis of the chain and crystalline structure of form 2. Eur Polym J. 1976;12:323–7.
11. Boor J, Mitchel JC. Apparent nucleation of a crystal-crystal transition in poly-1-butene. J Polym Sci. 1962;62:70–73.
12. Rubin I. Relative stabilities of polymorphs of polybutene-1 obtained from the melt. Polym Lett. 1964;2:747–9.
13. Holland VF, Miller RL. Isotactic polybutene-1 single crystals: morphology. J Appl Phys. 1964;35:3241–8.

14. Danusso F, Gianotti G. Isotactic polybutene-l : formation and transformation of modification 2. Makromol Chem. 1965;88:149–58.
15. Tosaka M, Kamijo T, Tsuji M, Kohjiya S, Ogawa T, Isoda S, Kobayashi T. High-resolution transmission electron microscopy of crystal transformation in solution-grown lamellae of isotactic polybutene-1. Macromolecules. 2000;33:9666–72.
16. Danusso F, Gianotti G, Polizzotti G. Isotactic polybutene-1: modification 3 and Its transformations. Die Makromol Chem. 1964;80:13–21.
17. Cojazzi J, Malta V, Celotti G, Zannetti R. Crystal structure of form III of isotactic poly-1-butene. Makromol Chem. 1976;177:915–26.
18. Danusso F, Gianotti G. The three polymorphs of isotactic polybutene-1 : dilatometric and thermodynamic fusion properties. Die Makromol Chem. 1963;61:139–56.
19. Clampitt BH, Hughes RH. Differential thermal analysis of polybutene-1. J Polym Sci Part C. 1964;6:43–51.
20. Maring D, Wilhelm M, Spiess HW, Meurer B, Weill G. Dynamics in the crystalline polymorphic forms I and II and form III of isotactic poly-1-butene. J Polym Sci Part B Polym Phys. 2000;38:2611–24.
21. Boor J Jr, Youngman EA. Polymorphism in poly-1-butene: apparent direct formation of modification I. J Polym Sci. 1964;2:903–7.
22. Rakus JP, Mason CDJ. The direct formation of modification I polybutene-1. Polym Sci Part B. 1966;4:467–8.
23. Schaffhauser RJ. On the nature of the form II to form I transformation in isotactic polybutene-1. J Polym Sci Part B Polym Phys. 1967;5:839–41.
24. Armeniades CD, Baer E. Effect of pressure on the polymorphism of melt crystallized polybutene-1. J Macromol Sci Part B Phys. 1967;1:309–34.
25. Nakafuku C, Miyaki T. Effect of pressure on the melting and crystallization behaviour of isotactic polybutene-1. Polymer. 1982;24:141–8.
26. Kopp S, Wittmann JC, Lotz B. Phase II to phase I crystal transformation in polybutene-1 single crystals: a reinvestigation. Polymer. 1994;35:916–24.
27. Nakamura K, Aoike T, Usaka K, Kanamoto T. Phase transformation in poly(1-butene) upon drawing. Macromolecules. 1999;32:4975–82.
28. Miyoshi T, Hayashi S, Imashiro F, Kaito A. Chain dynamics, conformations, and phase transformations for form III polymorph of isotactic poly (1-butene) investigated by high-resolution solid-state ^{13}C NMR spectroscopy and molecular mechanics calculations. Macromolecules. 2002;35:2624–32.
29. Miyoshi T, Hayashi S, Imashiro F, Kaito A. Side-chain conformation and dynamics for the form II polymorph of isotactic poly(1-butene) investigated by high-resolution solid-state ^{13}C NMR spectroscopy. Macromolecules. 2002;35:6060–3.
30. Fu Q, Heck B, Strobl G, Thomann YA. Temperature- and molar mass-dependent change in the crystallization mechanism of poly (1-butene): transition from chain-folded to chain-extended crystallization. Macromolecules. 2001;34:2502–11.
31. Yamashita M, Miyaji H, Hoshino A, Izumi K. Crystal growth of isotactic poly(butene-1) in the melt. I. Kinetic roughening. Polym J. 2004;36:226–37.
32. Yamashita M, Takahashi T. Melt crystallization of isotactic polybutene-1 trigonal form: the effect of side chain entropy on crystal growth kinetics. Polym J. 2008;40:996–1004.
33. Yamashita M. Regime II–III transition in isotactic polybutene-1 tetragonal crystal growth. Polymer. 2014;55:733–7.
34. Yamashita M, Hoshino A, Kato M. Isotactic poly(butene-1) trigonal crystal growth in the melt. J Polym Sci Part B Polym Phys. 2007;45:684–97.
35. Sasaguri K, Rhodes MB, Stein RS. Spherulite deformation in polybutene-1. Polym Lett. 1963;1:571–4.
36. Powers J, Hoffman JD, Weeks JJ, Quinn Jr. FA. Crystallization kinetics and polymorphic transformations in polybutene-1. J Res Nat Bur Stand A Phys Chem. 1965;69A:335–45.
37. Chau KW, Yang YC, Geil P. Tetragonal-twinned hexagonal crystal phase transformation in polybutene-1. J Mater Sci. 1986;21:3002–14.
38. Cavallo D, Gardella L, Portale G, Müller AJ, Alfonso G. Kinetics of cross-nucleation in isotactic poly(1-butene). Macromolecules. 2014;47:870–3.
39. Kajioka H, Taguchi K, Toda A. Cellular crystallization in thin melt film of it-poly(butene-1): an implication to spherulitic growth. Macromolecules. 2011;44:9239–46.
40. Qiao Y, Men Y. Intercrystalline links determined kinetics of form II to polymorphic transition in polybutene-1. Macromolecules. 2017;50:5490–7.
41. Patel GN, Patel RD. Growth mechanism of polymer hedrites. Eur Polym J. 1970;6:657–62.
42. Tashiro K, Hu J, Wang H, Hanesaka S, Alberto S. Refinement of the crystal structures of forms I and II of isotactic polybutene-1 and a proposal of phase transition mechanism between them. Macromolecules. 2016;49:1392–404.
43. Hu J, Tashiro K. Relation between higher-order structure and crystalline phase transition of oriented isotactic polybutene-1 investigated by temperature-dependent time-resolved simultaneous WAXD/SAXS measurements. Polymer. 2016;90:165–77.
44. Hu J, Tashiro K. Time-resolved imaging of the phase transition in the melt-grown spherulites of isotactic polybutene-1 as detected by the two-dimensional polarized IR imaging technique. J Phys Chem B. 2016;120:4689–98.
45. Fujiwara Y. II-I Phase transformation of melt-crystallized oriented Lamellae of polybutene-1 by shear deformation. Polym Bull. 1985;13:253–8.
46. Su F, Li X, Zhou W, Chen W, Li H, Cong Y, Hong Z, Qi Z, Li L. Accelerating crystal-crystal transition in poly(1-butene) with two-step crystallization: an in-situ microscopic infrared imaging and microbeam X-ray diffraction study. Polymer. 2013; 54:3408–16.
47. Su F, Li X, Zhou W, Zhu S, Ji Y, Wang Z, Qi Z, Li L. Direct formation of isotactic poly(1-butene) form I crystal from memorized ordered melt. Macromolecules. 2013;46:7399–405.
48. Chen W, Li X, Li H, Su F, Zhou W, Li L. Deformation-induced crystal–crystal transition of polybutene-1: an in situ FTIR imaging study. J Mater Sci. 2013;48:4925–33.
49. Kajioka H, Yoshimoto S, Gosh RC, Taguchi K, Tanaka S, Toda A. Microbeam X-ray diffraction of non-banded polymer spherulites of it-polystyrene and it-poly(butene-1). Polymer. 2010;51:1837–44.
50. Tashiro K, Yoshioka T, Yamamoto H, Wang H, Woo EM, Funaki K, Murase H. Re-investigation of Lamellar Aggregation State in Polyester Spherulites by means of Synchrotron X-ray Microbeam: the Lamellae are twisted or not? Polym Prep Jpn. 2014;63:1315–6.
51. Kikuzuki T, Shinobara Y, Nozue Y, Ito K, Amemiya Y. Determination of Lamellar twisting manner in a banded spherulite with scanning microbeam X-ray scattering. Polymer. 2010;51:1632–8.
52. Kolb R, Wutz C, Stribeck N, von Krosigk G, Riekel C. Investigation of secondary crystallization of polymers by means of microbeam X-ray scattering. Polymer. 2001;42:5257–66.
53. Murthy NS. Recent developments in polymer characterization using X-ray diffraction. Rigaku J. 2004;21:15–24.
54. Breedon JE, Jackson JF, Marcinkowski MJ, Taylor ME Jr. Study of Polyethylene spherulites using scanning electron microscopy. J Mater Sci. 1973;8:1071–82.

55. Bassett DC, Hodge AM. On Lamellar Organization in Banded Spherulites of Polyethylene. PolymER. 1978;19:469–72.
56. Lustiger A, Lotz B, Duff TS. The morphology of the spherulitic surface in polyethylene. J Polym Sci Polym Phys. 1989;27:561–79.
57. Kunz M, Drechsler M, Möller M. Gelation crystallized ultra-high molecular weight polyethylene: 1. Structure in swollen and dried gels. Polymer. 1995;36:1331–9.
58. Keith HD. Banding in spherulites: two recurring topics. Polymer. 2001;42:09987–93.
59. Keith HD, Padden FJ. Banding in polyethylene and other spherulites. Macromolecules. 1996;29:7776–86.
60. Li Y, Huang H, He T, Wang Z. Rhythmic growth combined with Lamellar twisting induces poly(ethylene adipate) nested ring-banded structures. ACS Macro Lett. 2012;1:154–8.
61. Wang T, Wang H, Li H, Gan Z, Yan S. Banded spherulitic structures of poly(ethylene adipate), poly(butylene succinate) and in their blends. Phys Chem Chem Phys. 2009;11:1619–27.
62. Woo EM, Wang LY, Nurkhamidah S. Crystal Lamellae of opposite orientations by three-dimensional dissecting onto spherulites of poly(ethylene adipate) crystallized in bulk form. Macromolecules. 2012;45:1375–83.
63. Woo EM, Wu PL, Wu MC, Yan KC. Thermal behavior of ring-band vs. maltese-cross spherulites: case in monomorphic poly(ethylene adipate). Macromol Chem Physic. 2006; 207:2232–43.
64. Donnay JDH, Harker D. A new law of crystal morphology extending the Law of Bravais. Am Mineral. 1937;22:446–67.
65. Massaro FR, Moret M, Bruno M, Rubbo M, Aquilano D. Equilibrium and growth morphology of oligoacenes: periodic bond chains (PBC) analysis of tetracene crystal. Cryst Growth Des. 2011;11:4639–46.
66. Carr JM, Langhe DS, Ponting MT, Hiltner A, Baer E. Confined crystallization in polymer nanolayered films: a review. J Mater Res. 2012;27:1326–50.